

NASA/TM—2003–104606, Vol. 24



**Technical Report Series on Global Modeling
and Data Assimilation**

Volume 24

**Temperature Data Assimilation with Salinity Corrections:
Validation for the NSIPP Ocean Data Assimilation System
in the Tropical Pacific Ocean, 1993-1998**

A. Troccoli, M.M. Rienecker, C.L. Keppenne, and G.C. Johnson

The NASA STI Program Office ... in Profile

Since its founding, NASA has been dedicated to the advancement of aeronautics and space science. The NASA Scientific and Technical Information (STI) Program Office plays a key part in helping NASA maintain this important role.

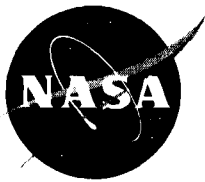
The NASA STI Program Office is operated by Langley Research Center, the lead center for NASA's scientific and technical information. The NASA STI Program Office provides access to the NASA STI Database, the largest collection of aeronautical and space science STI in the world. The Program Office is also NASA's institutional mechanism for disseminating the results of its research and development activities. These results are published by NASA in the NASA STI Report Series, which includes the following report types:

- **TECHNICAL PUBLICATION.** Reports of completed research or a major significant phase of research that present the results of NASA programs and include extensive data or theoretical analysis. Includes compilations of significant scientific and technical data and information deemed to be of continuing reference value. NASA's counterpart of peer-reviewed formal professional papers but has less stringent limitations on manuscript length and extent of graphic presentations.
- **TECHNICAL MEMORANDUM.** Scientific and technical findings that are preliminary or of specialized interest, e.g., quick release reports, working papers, and bibliographies that contain minimal annotation. Does not contain extensive analysis.
- **CONTRACTOR REPORT.** Scientific and technical findings by NASA-sponsored contractors and grantees.
- **CONFERENCE PUBLICATION.** Collected papers from scientific and technical conferences, symposia, seminars, or other meetings sponsored or cosponsored by NASA.
- **SPECIAL PUBLICATION.** Scientific, technical, or historical information from NASA programs, projects, and mission, often concerned with subjects having substantial public interest.
- **TECHNICAL TRANSLATION.** English-language translations of foreign scientific and technical material pertinent to NASA's mission.

Specialized services that complement the STI Program Office's diverse offerings include creating custom thesauri, building customized databases, organizing and publishing research results . . . even providing videos.

For more information about the NASA STI Program Office, see the following:

- Access the NASA STI Program Home Page at <http://www.sti.nasa.gov/STI-homepage.html>
- E-mail your question via the Internet to help@sti.nasa.gov
- Fax your question to the NASA Access Help Desk at (301) 621-0134
- Telephone the NASA Access Help Desk at (301) 621-0390
- Write to:
NASA Access Help Desk
NASA Center for AeroSpace Information
7121 Standard Drive
Hanover, MD 21076-1320



**Technical Report Series on Global Modeling
and Data Assimilation**

Volume 24

**Temperature Data Assimilation with Salinity Corrections:
Validation for the NSIPP Ocean Data Assimilation System
in the Tropical Pacific Ocean, 1993-1998**

*Alberto Troccoli, Michele M. Rienecker
Goddard Space Flight Center, Greenbelt, MD*

*Christian L. Keppenne
Science Applications International Corporation, Beltsville, MD*

*Gregory C. Johnson
National Oceanic & Atmospheric Administration, Seattle, WA*

National Aeronautics and
Space Administration

Goddard Space Flight Center
Greenbelt, Maryland 20771

Available from:

NASA Center for AeroSpace Information
7121 Standard Drive
Hanover, MD 21076-1320
Price Code: A17

National Technical Information Service
5285 Port Royal Road
Springfield, VA 22161
Price Code: A10

ABSTRACT

The NASA Seasonal-to-Interannual Prediction Project (NSIPP) has developed an ocean data assimilation system to initialize the quasi-isopycnal ocean model used in our experimental coupled-model forecast system. Initial tests of the system have focused on the assimilation of temperature profiles in an optimal interpolation framework. It is now recognized that correction of temperature only often introduces spurious water masses. The resulting density distribution can be statically unstable and also have a detrimental impact on the velocity distribution. Several simple schemes have been developed to try to correct these deficiencies. Here the salinity field is corrected by using a scheme which assumes that the temperature-salinity relationship of the model background is preserved during the assimilation. The scheme was first introduced for a z-level model by Troccoli and Haines (1999). A large set of subsurface observations of salinity and temperature is used to cross-validate two data assimilation experiments run for the 6-year period 1993-1998. In these two experiments only subsurface temperature observations are used, but in one case the salinity field is also updated whenever temperature observations are available.

The effectiveness of the Troccoli and Haines scheme is reflected not only in a better salinity field but also in an improved temperature field. The root-mean-square difference (RMSD) between the assimilation analyses and observations in the equatorial Pacific shows an average improvement in the upper 900m of 20% in the salinity field and of 6% in the temperature field. The impact of the subsurface assimilation has been also assessed via data retention experiments (simulated forecasts). The RMSD diagnostic for these “forecasts” increases only moderately up to a 6-month lead, showing the retention for several months of information from the assimilation.

TABLE OF CONTENT

1. INTRODUCTION.....	(1)
2. THE MODEL AND ASSIMILATION SYSTEM.....	(2)
2.1 <i>The ocean model</i>	(2)
2.2 <i>Model setup</i>	(3)
2.3 <i>Data Assimilation System</i>	(4)
2.4 <i>Salinity increments to preserve water-mass distributions</i>	(5)
2.5 <i>Incremental analysis</i>	(7)
2.6 <i>Description of the assimilation experiments</i>	(7)
3. COMPARISON WITH SUBSURFACE OBSERVATIONS	(7)
3.1 <i>The 155 °W section</i>	(8)
3.2 <i>Cross-validation statistics</i>	(12)
3.3 <i>Temperature-Salinity Relations</i>	(14)
4. DATA RETENTION	(16)
5. SUMMARY AND DISCUSSION	(18)
ACKNOWLEDGEMENTS	(19)
REFERENCES.....	(21)

List of Figures

1. Horizontal domain decomposition for the Pacific model. The thin lines delineate grid cells. The thick lines correspond to the boundaries of each Processing Element (PE) on a 16×16 PE lattice. The dark circles show the locations of the TAO moorings. (4)
2. Schematic representation of the two analyses (right) obtained by combining model and XBT water columns for the monotonic-profile case, following TH99. The shaded layers in the lower analysis profile highlight unstable water masses introduced by the vertical displacement of the temperature profile without corresponding displacement of the salinity profile. θ is potential temperature. (6)
3. Observation locations are denoted by the rectangles whose vertical sides are proportional to the latitudinal extent of the transects. The horizontal line inside the rectangle identifies the equator. The crosses indicate a subset of the transects occupied in April-September and used for data retention experiments. There are 69 transects in total, of which 35 are used for the data retention experiments. (8)
4. Meridional sections of temperature across the equator at 155°W for Johnson *et al.* (2000) (JMRM), *TOI*, *TOIS* and *CNT* for the five months presented by JMRM (cf. JMRM's plate 2). The equator is highlighted in white. Isolines are thicker for 8, 18 and 28°C (10)
5. As in Figure 4 but for salinity. Isolines are thicker for 34, 35 and 36. (11)
6. Root-mean-square difference (RMSD) between the three model runs (*TOI*, *TOIS* and *CNT*) and the observations as a function of depth for the 69 available transects in Figure 3: west equatorial Pacific (a, c) and east equatorial Pacific (b, d); temperature RMSD (a-b) and salinity RMSD (c-d). (13)
7. Temperature-Salinity diagrams for *TOI*, *TOIS* and observations (OBS) for the four regions defined on each panel. The color convention is explained in panel c. For instance, the red color means that both *TOI* and *TOIS* agree with observations. Superimposed dotted lines are the σ isolines. (15)
8. As in Figure 6 but for the two assimilation runs, *TOI* and *TOIS*, and the two simulated forecasts, f_TOI and f_TOIS , and for the 35 crossed transects (see Figure 3). (17)
9. Temporal evolution of the composite RMSD of the 19°C isotherm depth (a-b) and of the salinity on the 25 sigma surface (c-d) for all lead times for the control run (*CNT*), the two assimilation runs (*TOI* and *TOIS*), and the simulated forecasts (f_TOI and f_TOIS). The RMSD calculation is split in south (a, c) and north (b, d) of the equator. (18)

1. Introduction

Assimilation of subsurface temperature (T) observations has improved the quality of ocean state analyses. When these analyses are used to initialize coupled-model predictions, the forecast skill also improves (e.g., Ji *et al.*, 1998, and Segsneider *et al.*, 2001). However, it has been shown that the univariate assimilation of temperature has deleterious effects on the salinity (S) field and hence on the density field (Cooper, 1988, Acero-Schertzer *et al.*, 1997, Ji *et al.*, 2000, Troccoli *et al.*, 2002, the latter hereafter referred to as TBS02).

Some solutions to this problem have already been put forward. The proposed solutions can be broadly divided into two main categories: those that rely on direct observations in order to construct some historical correction (Vossepoel *et al.*, 1999, Maes and Behringer, 2000, and Vossepoel and Behringer, 2000) and those that draw statistical or physical information from the model itself [e.g., through an Ensemble Kalman Filter (EnKF: Keppenne and Rienecker, 2002) or model statistics, or from local model background water mass properties as in Troccoli and Haines, (1999), hereafter TH99]. Given the scarcity of direct salinity measurements, applications of the first approach are necessarily limited as their training period can only refer to restricted time-space intervals. This restriction reflects on the limited variability contained in the statistics. This situation appears unlikely to change for a few years to come, although efforts for a better salinity observing network are underway, especially with Argo floats (e.g., <http://www.argo.ucsd.edu>). On the other hand, the more complex primitive equation models, such as the HOPE model at the European Centre for Medium-Range Weather Forecasts (ECMWF, see TBS02) and the Poseidon model at the NASA Seasonal-to-Interannual Prediction Project (NSIPP, see Coles and Rienecker, 2001), have proven capable of simulating the water-mass characteristics quite well. This has allowed the development of methods belonging to the second category. However, it is one of the objectives of this paper to further validate the water-mass characteristics of the Poseidon model using a substantial number of subsurface observations.

In this work, as in TBS02, the focus is on the use of model-derived water-mass properties (T and S) to correct the model salinity commensurate with the temperature corrections made by assimilating temperature observations. The salinity increments are calculated according to the temperature analysis by preserving the model's local T - S relationships as described in TH99. The TH99 (salinity) scheme does not make any use of statistics for the salinity adjustment. Two other appealing advantages of this approach are computational costs and model portability.

An initial evaluation of the TH99 scheme, using a z -coordinate ocean model, was presented in TBS02. Subsequently, Segsneider *et al.* (2001) showed that when the TH99 scheme is added to their combined temperature and sea surface height assimilation, it improves the ECMWF seasonal forecast on lead times greater than 3 months, and up to 6 months. The same scheme is implemented here in a quasi-isopycnal model to test whether a different model formulation would also benefit from the TH99 scheme. The validation of the TH99 scheme, undertaken in TBS02 by a comparison with climatologies, is extended here through a comparison with an abundant set of independent (i.e., not assimilated) observations and by using different diagnostics. As a further step, the retention of information - either improved or degraded structure, depending on whether salinity is adjusted or not - is assessed in simulated forecast mode, that is, when the assimilation ceases but the prescribed time-dependent forcing is continued. This experiment has the advantage

over coupled forecast tests in that the shock or drift usually found to dominate initial evolution of coupled models is not present to confuse the interpretation of results.

In section 2 the ocean model, the data assimilation system and the experiments are described. Comparisons with comprehensive observation analyses are presented in section 3 for the assimilation experiments. In section 4, the simulated forecasts are analyzed. Finally, a discussion is presented in section 5.

2. The Model and Assimilation System

2.1 The ocean model

The ocean model used in this study is the reduced-gravity quasi-isopycnal Poseidon ocean model, Version 4, which uses a generalized vertical coordinate designed to represent a turbulent, well-mixed surface layer and nearly isopycnal deeper layers. Coastal topography is represented, but the reduced-gravity treatment precludes the use of variable bottom depth. Poseidon has been documented and validated in hindcast studies of El Niño (Schopf and Loughe, 1995) and has since been updated to include prognostic salinity (*e.g.*, Yang *et al.*, 1999). More recently, the model has been used in an investigation of the annual cycle in the eastern Equatorial Pacific (Yu *et al.*, 1997) and in a numerical study of the surface heat balance along the equator (Borovikov *et al.*, 2001).

Poseidon's prognostic variables are layer thickness, $h(\lambda, \theta, \zeta, t)$, temperature, $T(\lambda, \theta, \zeta, t)$, salinity, $S(\lambda, \theta, \zeta, t)$, and the zonal and meridional current components, $u(\lambda, \theta, \zeta, t)$ and $v(\lambda, \theta, \zeta, t)$, where λ is longitude, θ latitude, t time and ζ is a generalized vertical coordinate which is 0 at the surface and increments by 1 between successive layer interfaces.

Explicit detail of the model, its vertical coordinate representation and its discretization are provided in Schopf and Loughe (1995) and are only summarized here. The equation for mass continuity is

$$\frac{\partial h}{\partial t} + \nabla \cdot (\mathbf{v}h) + \frac{\partial w_e}{\partial \zeta} = 0, \quad (2.1.1)$$

where $\nabla \cdot$ and \mathbf{v} are the two-dimensional (2D) divergence operator and velocity vector and w_e represents the volume flux across layer interfaces, including freshwater flux through the surface.

The heat equation is

$$\frac{\partial hT}{\partial t} + \nabla \cdot (\mathbf{v}hT) + \frac{\partial w_e T}{\partial \zeta} = \frac{\partial}{\partial \zeta} \left(\frac{\kappa}{h} \frac{\partial T}{\partial \zeta} \right) + \frac{\partial Q}{\partial \zeta} + hF_h(T), \quad (2.1.2)$$

where Q is the external heat flux, κ is a heat diffusivity and F_h is a 2D smoothing operator. The salinity equation is

$$\frac{\partial hS}{\partial t} + \nabla \cdot (\mathbf{v}hS) + \frac{\partial w_e S}{\partial \zeta} = \frac{\partial}{\partial \zeta} \left(\frac{\kappa_s}{h} \frac{\partial S}{\partial \zeta} \right) + hF_h(S), \quad (2.1.3)$$

where κ_s is a salinity diffusivity. The 2D momentum equation is

$$\frac{\partial(\mathbf{v}h)}{\partial t} + \nabla \cdot (\mathbf{v}h\mathbf{v}) + \frac{\partial w_e \mathbf{v}}{\partial \zeta} = -\frac{h}{\rho_0} \nabla p' - bh\nabla z - f \mathbf{k} \times \mathbf{v} + \frac{\partial}{\partial \zeta} \left(\frac{\nu}{h} \frac{\partial \mathbf{v}}{\partial \zeta} \right) + \frac{1}{\rho_0} \frac{\partial \tau}{\partial \zeta} + hF_v(\mathbf{v}), \quad (2.1.4)$$

where ν is a vertical friction, τ is the vertical shear stress, $f\mathbf{k} \times \mathbf{v}$ is the Coriolis acceleration and F_v is a dissipation term. A hydrostatic Boussinesq approximation is made, so that if $p'(z)$ is the pressure anomaly at depth z , b is buoyancy and ρ_0 is the mean density, the hydrostatic equation then becomes

$$\frac{\partial p'}{\partial \zeta} = -\rho_0 bh. \quad (2.1.5)$$

Following Pacanowski and Philander (1981), vertical mixing is parameterized through a Richardson number-dependent mixing scheme implemented implicitly. An explicit mixed layer is included with a mixed layer entrainment parameterization following Niiler and Kraus (1977).

A time-splitting integration scheme is used whereby the hydrodynamics are done with a short time step (15 minutes), but the vertical diffusion, convective adjustment and filtering are done with coarser time resolution (half-daily).

2.2 Model setup

The version of Poseidon used here has been parallelized as in Konchady *et al.* (1998) using the same message-passing protocol and 2D horizontal domain decomposition used by Schaffer and Suarez (2000) for the atmospheric model. Many of the details of the parallel implementation of both the model and the assimilation system can be found in Keppenne and Rienecker (2001).

The model, in a global configuration, is used for NSIPP's coupled forecast system. However, for this study the domain was restricted to the Pacific Ocean, from 45°S to 60°N. The horizontal resolution was $1^\circ \times 1^\circ$, plus an equatorial refinement: the meridional resolution changes smoothly from $1/3^\circ$ at the equator to 1° within 10° of the equator (Figure 1). There are 20 layers in the vertical. At the southern boundary temperature and salinity are relaxed towards the Levitus climatology. There are $173 \times 164 \times 20$ grid boxes, of which 28% are situated over land.

The model is forced by daily averaged wind stresses derived from the Special Sensor Microwave/Imager (SSM/I) by Atlas *et al.* (1996). The same wind product, but monthly averaged, is used to derive the sensible and latent heat components through the atmospheric mixed layer model by Seager *et al.* (1995). The precipitation is given by the monthly averaged analyses of Xie and Arkin (1997). An additional relaxation to climatology is applied to the surface salinity field with a time scale of nine months.

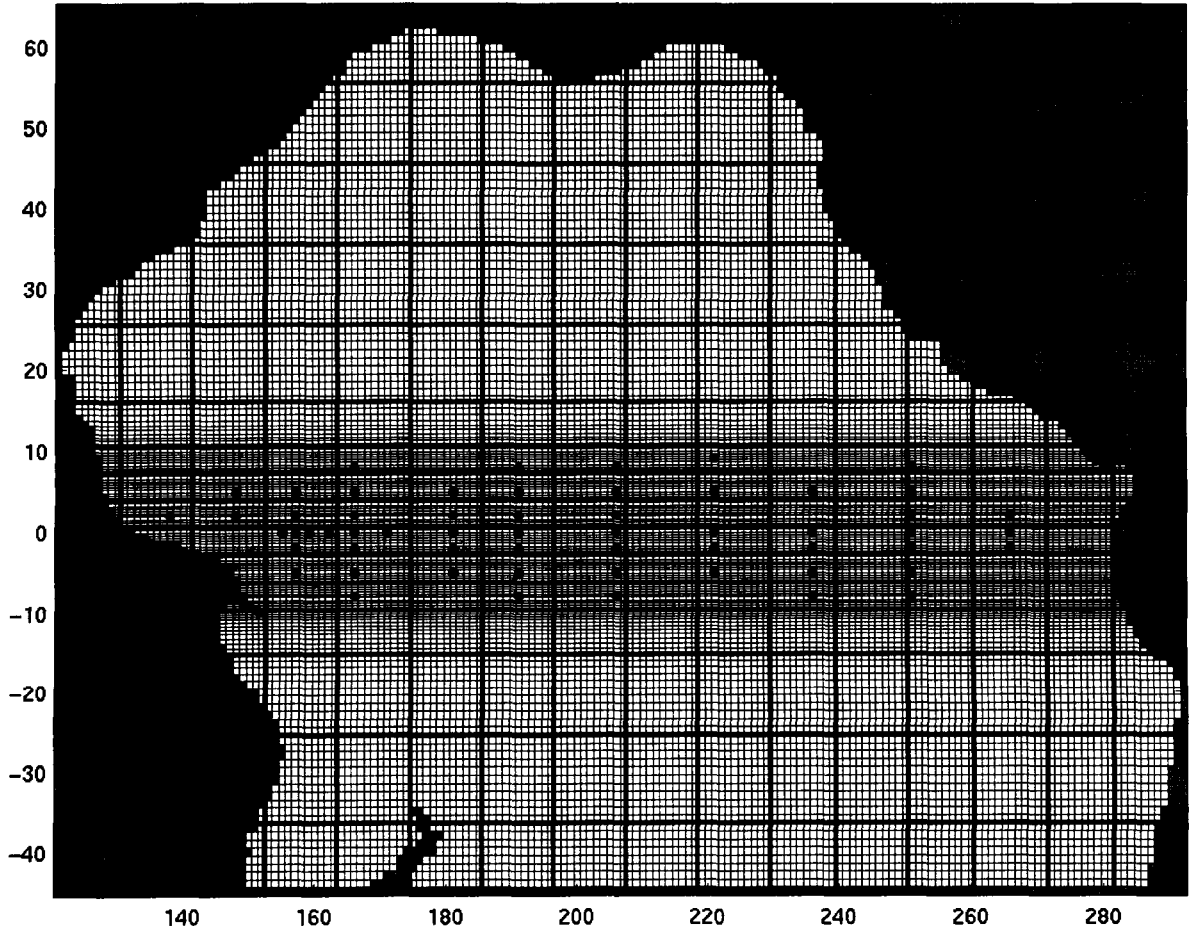


Figure 1. Horizontal domain decomposition for the Pacific model. The thin lines delineate grid cells. The thick lines correspond to the boundaries of each Processing Element (PE) on a 16×16 PE lattice. The dark circles show the locations of the TAO moorings.

2.3 Data Assimilation System

The data assimilation system in this study is composed of two parts: a univariate optimal interpolation system (UOI) to calculate the temperature analysis increments, followed by the TH99 scheme to calculate salinity increments consistent with the temperature analysis. The temperature analysis is generated according to

$$[\mathbf{HP}^f \mathbf{H}^T + \mathbf{W}] \mathbf{b} = \mathbf{d} - \mathbf{H} \mathbf{x}^f, \quad (2.3.1)$$

$$\mathbf{x}^a = \mathbf{x}^f + \mathbf{P}^f \mathbf{H}^T \mathbf{b}. \quad (2.3.2)$$

In (2.3.1) and (2.3.2), uppercase boldface symbols represent matrices, and lowercase boldface symbols represent vectors. The vector \mathbf{d} ($n_d \times 1$) contains n_d observations; \mathbf{x} ($n_x \times 1$) is the state vector. The superscripts a and f refer to the analyzed state and the forecast, respectively. The matrix \mathbf{W} ($n_d \times n_d$) is the observational error covariance matrix. The representer matrix,

$\mathbf{R} = \mathbf{H}\mathbf{P}^f\mathbf{H}^T$, maps the background (forecast) error covariance matrix, \mathbf{P}^f ($n_x \times n_x$), to the error subspace of the measurements. The elements of \mathbf{b} are the representer-function amplitudes used to update \mathbf{x} . The $n_d \times 1$ vector, $\mathbf{z} = \mathbf{d} - \mathbf{H}\mathbf{x}^f$, contains the innovations.

In this application, the measurement functional, $\mathbf{H}\mathbf{x}$, is simply a 3D interpolation operator which maps the model temperature field, assumed to be at the center of the model layer, to the latitude, longitude and depth of each observation. The background-error covariance used in the UOI is constant in time. Here the function depends only on the distance between forecast locations, and a Gaussian functional form is chosen:

$$\mathbf{P}^f(\Delta\lambda, \Delta\phi, \Delta z) = C \exp\{-(\Delta\lambda/L_\lambda)^2 - (\Delta\phi/L_\phi)^2 - (\Delta z/L_z)^2\},$$

where L_λ defines the zonal decorrelation scale, L_ϕ the meridional decorrelation scale and L_z the vertical decorrelation scale. In this application, $L_\lambda = 1800$ km, $L_\phi = 400$ km in the equatorial waveguide, and $L_z = 50$ m. The horizontal scales are consistent with those used by Ji *et al.* (1995). The value for L_λ is modulated meridionally as suggested by Derber and Rosati (1989) to shorten the covariance scales with latitude.

2.4 Salinity increments to preserve water-mass distributions.

Troccoli and Haines (1999) demonstrated the deleterious effects of assimilating temperature profiles without making corresponding adjustments to the salinity profile at each model grid point influenced by the temperature assimilation. The problems arise from the introduction of gravitationally unstable profiles through the generation of new water masses (e.g., Figure 2). They proposed a scheme to preserve the water-mass distribution of the model prior to assimilation. The idea stems from the fact that vertical displacements of the water column, because of internal wave motion or the passage of mesoscale features, can occur without significant changes in the water mass properties. Even for the case of non-monotonic $S=S(T)$, two (or more) isothermic parcels can be distinguished according to their depth and the TH99 scheme recovers salinity from the nearest $T(z)$ in the background field.

The scheme is presented fully in TH99 and TBS02 and is presented only briefly here. The procedure is applied at each model grid point in two steps. First, a vertical displacement of the model T background profile to match the deepest analyzed T is made. The same displacement is applied to the S profile, too. Second, the scheme computes an S increment using the T - S relationships from the model T - and S -background profiles and the analyzed T , at each grid point, according to the following formulation:

$$\begin{aligned} S(z_{an}) &= S_{bg}(z_{bg}) && \text{if } |z_{an} - z_{bg}| \leq \Delta z \\ S(z_{an}) &= S_{bg}(z_{an}) && \text{if there is no } z_{bg} \text{ such that } T_{bg}(z_{bg}) = T_{an}(z_{an}), \\ &&& \text{or } |z_{an} - z_{bg}| > \Delta z \end{aligned}$$

where Δz is a specified depth tolerance, which could be a function of location. In our case we chose a fixed $\Delta z = 100$ m. Subscripts *an* and *bg* stand for analysis and background, respectively, and $z_{bg} = z(T_{bg} = T_{an})$ is the depth at which the background temperature is the same as the analysis

temperature. In case of multiple $z(T_{bg}=T_{an})$ solutions, the nearest depth to z_{an} is considered. Also, as the T - S preservation assumption generally does not hold near the surface, the salinity is not updated in the surface isothermal layer.

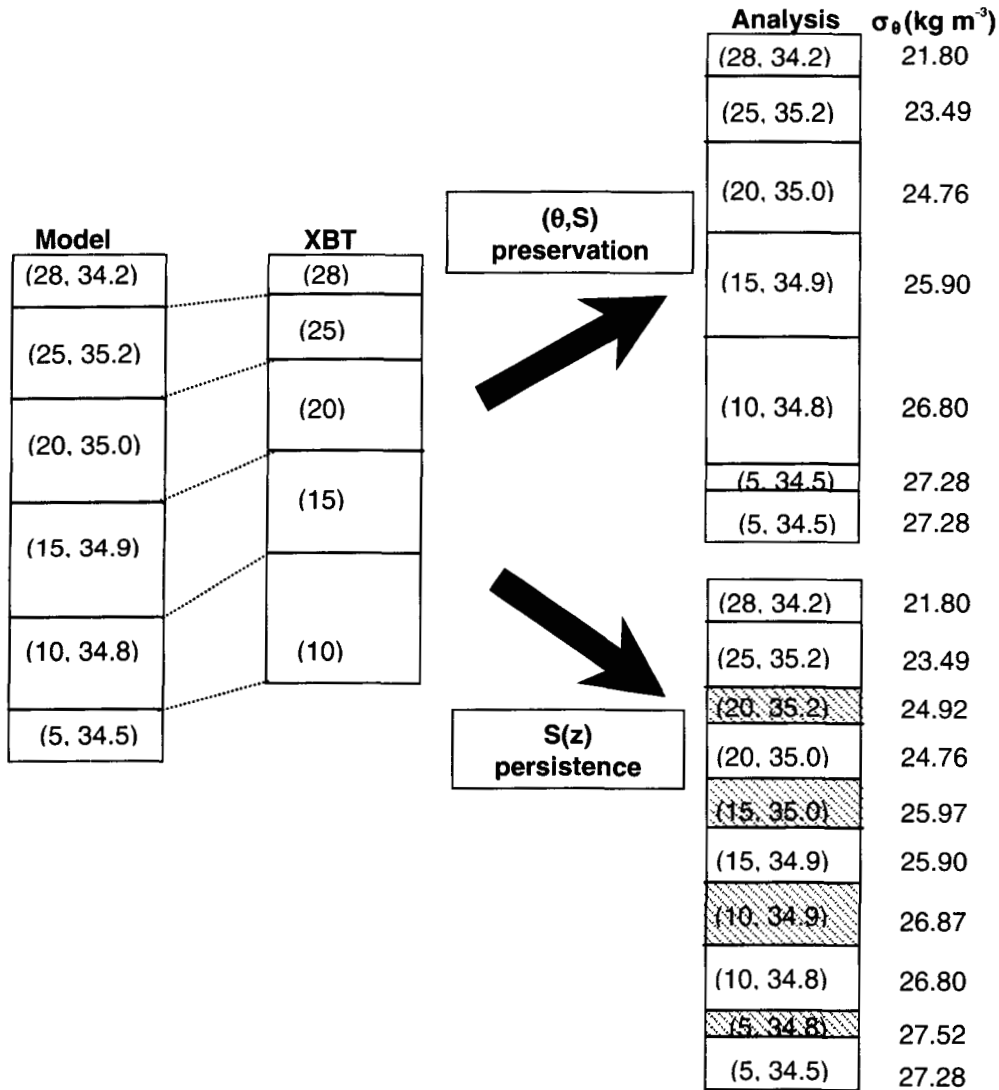


Figure 2. Schematic representation of the two analyses (right) obtained by combining model and XBT water columns for the monotonic-profile case, following TH99. The shaded layers in the lower analysis profile highlight unstable water masses introduced by the vertical displacement of the temperature profile without corresponding displacement of the salinity profile. θ is potential temperature.

Thus, the TH99 scheme only needs three easily retrievable ingredients: (1) the analyzed temperature profile, (2) the model temperature, and (3) salinity profiles for each model grid point. The analyzed temperature profile can be the result of any analysis method such as optimal interpolation.

2.5 Incremental analysis

Incremental analysis updating (IAU, e.g., Bloom *et al.* 1996) is used to insert the analysis increments, $\mathbf{x}^a - \mathbf{x}^f$, into the model in a gradual manner. Namely, the model partial differential equations (2.1.1-2.1.4) are replaced with

$$\frac{\partial \mathbf{x}}{\partial t} = \mathbf{F}(\mathbf{x}, t) + \frac{(\mathbf{x}^a(t_i) - \mathbf{x}^f(t_i))}{(t_{i+1} - t_i)}, \quad t_i \leq t < t_{i+1}, \quad (2.5.1)$$

where \mathbf{F} stands for the right hand sides of (2.1.2-2.1.3) and $\mathbf{x}^a(t_i)$ and $\mathbf{x}^f(t_i)$ are the analysis and forecast at the time, t_i , of the i th analysis.

Unlike nudging (e.g., Daley 1991), which relaxes the model state toward an analysis, the analysis increments are inserted as a state-independent forcing term. The IAU has properties similar to those of a low-pass filter and can improve observed-minus-forecast statistics with respect to a non-incremental updating scheme (Bloom *et al.* 1996).

The IAU is used here for two reasons. First, it lessens the unwanted effects of intermittent data assimilation, specifically initialization shocks resulting from imbalances between the model fields following the direct insertion of the analysis increments. Second, the IAU allows the model to gradually adjust the h field in response to the T and S increments without violating the constraints imposed by the continuity equation (2.1.1).

2.6 Description of the assimilation experiments.

The subsurface temperature measurements employed in this study include all the observations available in real-time from the Global Telecommunication System, including XBTs (eXpendable BathyThermographs), TAO (Tropical Atmosphere-Ocean) mooring data (e.g., McPhaden *et al.*, 1998), and profiling floats. The observations were quality controlled at the National Center for Environmental Prediction (NCEP). Two experiments have been run to examine the ocean structure evolution. For the first, only temperature is updated (experiment *TOI*). For the second, salinity as well as temperature is updated (experiment *TOIS*), with the salinity increments given by the TH99 scheme. For reference, a control run with no data assimilation (experiment *CNT*) is used to check how the data assimilation affects systematic model errors. The three runs all use the ocean model set-up described in section 2.2. The initial conditions were taken from a spun up simulation where climatological forcing was applied for 10 years and then daily forcing from 1988 onwards. The experiments in this study were run for the 6-year period 1993-1998.

3. Comparison with subsurface observations

Subsurface salinity observations are rather scarce and so it is generally difficult to validate model and/or assimilation results in terms of the salinity field. A recent paper by Johnson *et al.* (2000) (hereafter JMRM) provided a thorough data analysis of salinity from Conductivity-Temperature-Depth (CTD) observations for the equatorial Pacific for the period from September 1996 to

November 1998. That dataset has since been extended. This study uses all the CTD observations available for the period 1993-1998. The transects are located in the zone between 165°E and 95°W and normally extend from 8°S to 8°N (see Figure 3). The temperature and salinity accuracies are 0.002°C and 0.003¹, respectively. The JMRM observations were mapped onto a high resolution grid with 1/5° meridional spacing and 10m vertical spacing. In the following, it should be borne in mind that the observed fields are gridded quasi-synoptic one-time sections whereas for the model fields we will consider monthly averages.

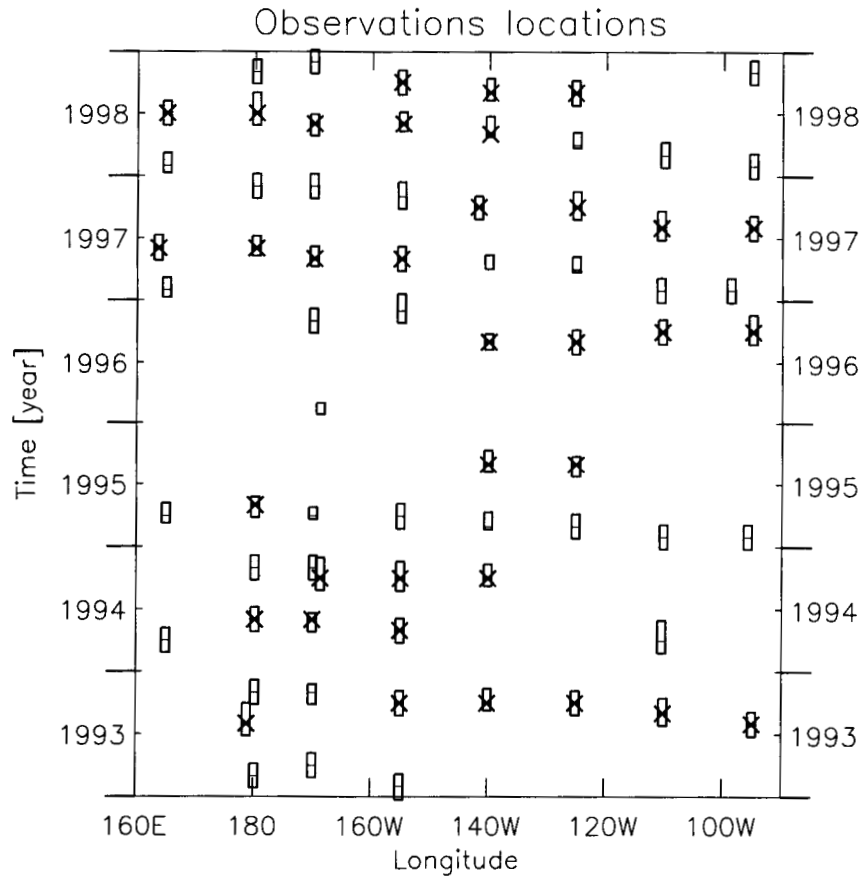


Figure 3. Observation locations are denoted by the rectangles whose vertical sides are proportional to the latitudinal extent of the transects. The horizontal line inside the rectangle identifies the equator. The crosses indicate a subset of the transects occupied in April-September and used for data retention experiments. There are 69 transects in total, of which 35 are used for the data retention experiments.

3.1 The 155°W section

The physical structures of the analyses from the different experiments have been compared with that from JMRM's analysis. Here, the focus is on the meridional section at 155°W. This choice is motivated by good temporal and spatial coverage (Figure 3), by location (the central Pacific), and by the strength of the salinity signal (there is a pronounced salinity tongue).

¹ Salinity is unitless, as defined by the 1978 Practical Salinity Scale.

Let us first consider the temperature field, retrieved from the same CTD casts as salinity, so as to appreciate the modifications introduced by the OI procedure. Figure 4 shows the meridional transects across the equator at 155°W for JMRM's analysis, *TOI*, *TOIS* and *CNT* (from left to right, respectively) for the five months presented by JMRM. We will mainly focus on two features: the vertical temperature gradient and the meridional thermocline gradient.

The thermocline is considerably tighter in the observation, than in the control run, *CNT*, especially in November 1997. Observed gradients are up to 1.5°C over 10m. In the *TOI* and *TOIS* assimilation runs the thermocline becomes tighter than in *CNT*, and hence closer to the observations. Yet, the vertical gradient in *TOI* and *TOIS* is not as strong as in the observations. The difference is mainly due to the fact that monthly averages of the model fields are being considered. In fact, other analyses have shown that the vertical displacement of the thermocline on even shorter time scales (about 10 days) can be as large as 40m or more, which can translate to a temperature variability of about 2.5°C (cf. Figure 2 in TH99). Similar considerations will also apply to the salinity field for which the same displacements can lead to a salinity variability of up to about 0.2.

Taking the 18°C isotherm as a reference, it can be seen that the meridional gradient of the thermocline is reasonably well simulated by the control run (compare the first and last columns of Figure 4). The main contribution of the assimilation runs is in the region of the pronounced thermocline ridge near 6-8°N where both meridional and vertical gradients are sharpened by the assimilation. Another feature worth noting is the bulge present in the 12°C isotherm in some of the *TOI* transects, such as at 4°S in December 1996 and at the equator in November 1997. We will come back to this point later in this section.

The salinity fields for the same five transects are presented in Figure 5. For the comparisons of salinity structure we focus on three regions: the subsurface both south (i.e., the salinity tongue) and north of the equator, and the upper water column. The shape of the salinity tongue is well captured by *CNT*. Even the excursions of the 35 isohaline across the equator during 1997 (an El Niño year) are reproduced reasonably well. However, the values are often 0.2-0.4 higher than observed. North of the equator, the subsurface salinity structure is rather uniform and close to observations, although north of about 4°, the observed values are normally underestimated by about 0.2 in the model. Near the surface, differences are less systematic. South of the equator, *CNT* is often saltier than observed; however, except for poleward of 4°S in November 1997, differences are within 0.2 to 0.4.

The salinity tongue comparison between *TOI* and *TOIS* shows that, although the high salinity values are present in both runs, the shape of the tongue is generally too diffuse in the *TOI* run. In comparison, *TOIS* captures the observed features better. Salty water observed in the lower thermocline is associated with eastward advection of salty water in the Equatorial Undercurrent (EUC). This contrasts with surrounding westward advection of fresher water in the South Equatorial Current (JMRM). Similar features but with a smaller magnitude are also present in *TOIS* and *CNT*. A striking feature is that in all the panels for the *TOI* run, a column of salty water ($S > 34.8$) extending a few hundred meters below the thermocline is prominent just south of the equator.

Temperature at 155°W

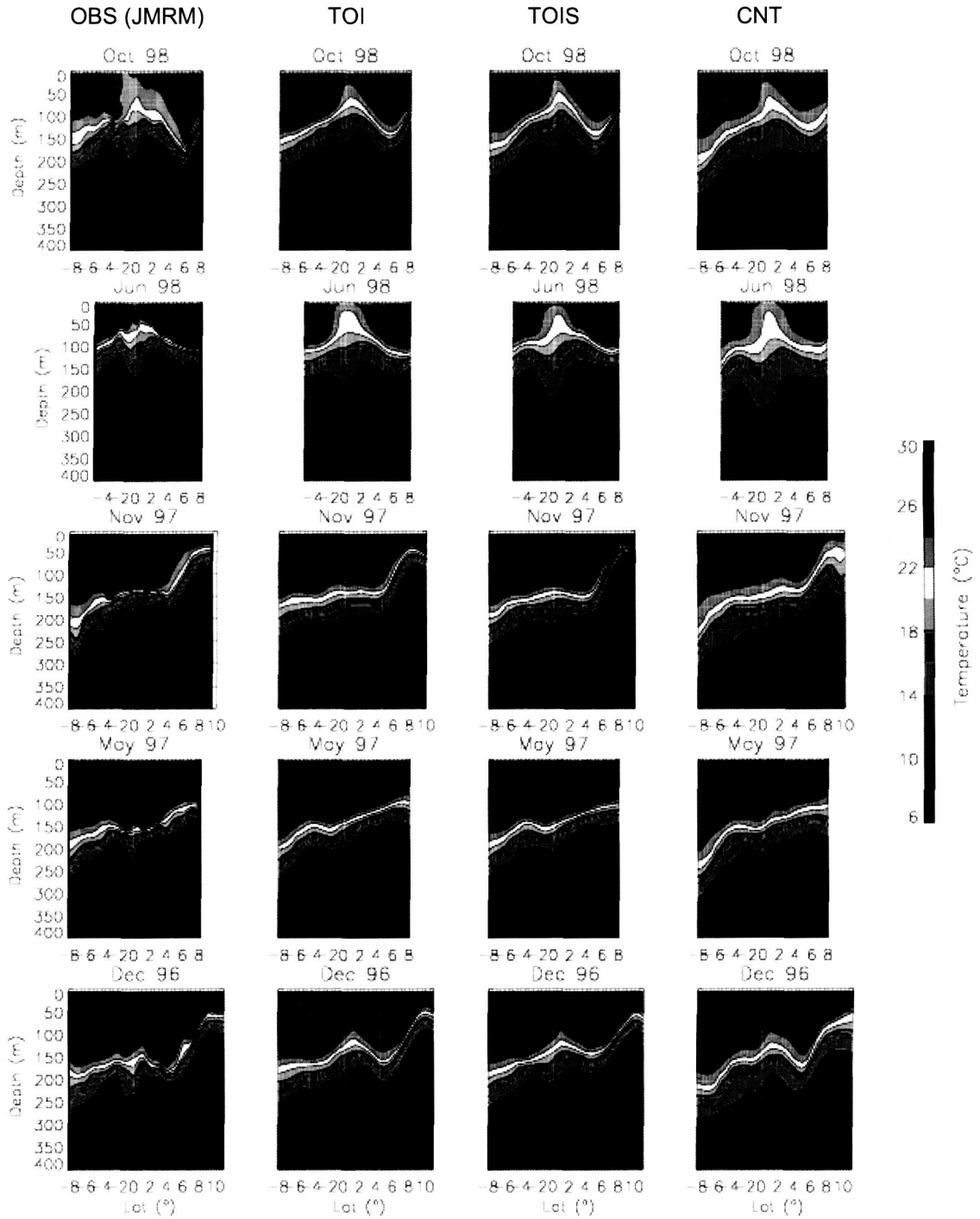


Figure 4: Meridional sections of temperature across the equator at 155°W for Johnson *et al.* (2000) (JMRM), *TOI*, *TOIS* and *CNT* for the five months presented by JMRM (cf. JMRM's plate 2). The equator is highlighted in white. Isolines are thicker for 8, 18 and 28°C.

Such features are common in cases in which temperature is assimilated with no salinity correction, in areas with a marked salinity gradient, as discussed by the stability analysis in TBS02. As a result, gravitationally unstable conditions, which cause warm and salty water to be entrained at depth, are spuriously introduced in the model. This is an undesirable feature as the spurious water mass may persist in the model for a long time. On the other hand, with *TOIS*, the marked columns of salty water seen in *TOI* have almost entirely disappeared and *TOIS* is closer in character to the observations.

North of the equator, *TOI* and *TOIS* do not differ much from each other and both suffer from a fresh bias. This bias, as observed earlier, is a legacy of the control run and therefore it is not possible to eliminate it with the adopted assimilation approach.

It is interesting to note that in *TOIS*, the near-surface salinity is generally better simulated than in both *CNT* and *TOI*, even though it is not corrected. This is probably a reflection of the improved subsurface salinity structure which may be entrained into the surface layer during mixing. In fact, the surface forcings are essentially the same as those in *TOI*, and differ from *CNT* solely by the evaporation component which, however, does not seem to play a dominant role (compare *TOI* and *CNT*). Note also that the three runs are all subject to the same sea surface salinity relaxation. Even the surface zonal current is reproduced better by *TOIS*.

3.2 Cross-validation statistics

A cross-validation against all available JMRM temperature and salinity observations was conducted by calculating the root-mean-square difference (RMSD) for the three runs (Figure 6). For each model variable we consider the nearest observation value. The 69 transects available are then grouped into two sets: west equatorial Pacific (WEP), for longitudes between 160°E and 150°W, and east equatorial Pacific (EEP) between 150°W and 90°W.

As expected, the temperature RMSD is notably reduced in the two assimilation runs with respect to the *CNT* run (Figures 6a, b). This reduction is more accentuated in the EEP, where the RMSD in *CNT* is larger, by more than 0.5°C, than in either *TOI* or *TOIS* in most of the thermocline, that is from 50m to 250m. The reduction is marked even in the WEP but the magnitude is generally halved. Some small differences appear also between *TOI* and *TOIS* at thermocline depths, with *TOIS* generally closer to observations, especially between 50m and 100m in the EEP where the two RMSD differ by up to 0.25°C. More important, however, are the differences between *TOI* and *TOIS* below 50m. This is especially valid for the EEP since in the WEP the differences are marginal. In the EEP, in fact, the differences reach about 0.3°C at 450m. The larger RMSD for *TOI* reflects the worsening of the thermal structure below the thermocline as a consequence of the instabilities introduced as discussed above. Therefore, it is a positive feature of the TH99 scheme that by changing the salinity field, even the thermal structure is improved. The *TOIS* reduces the temperature RMSD with respect to *CNT* by a considerable 17%.

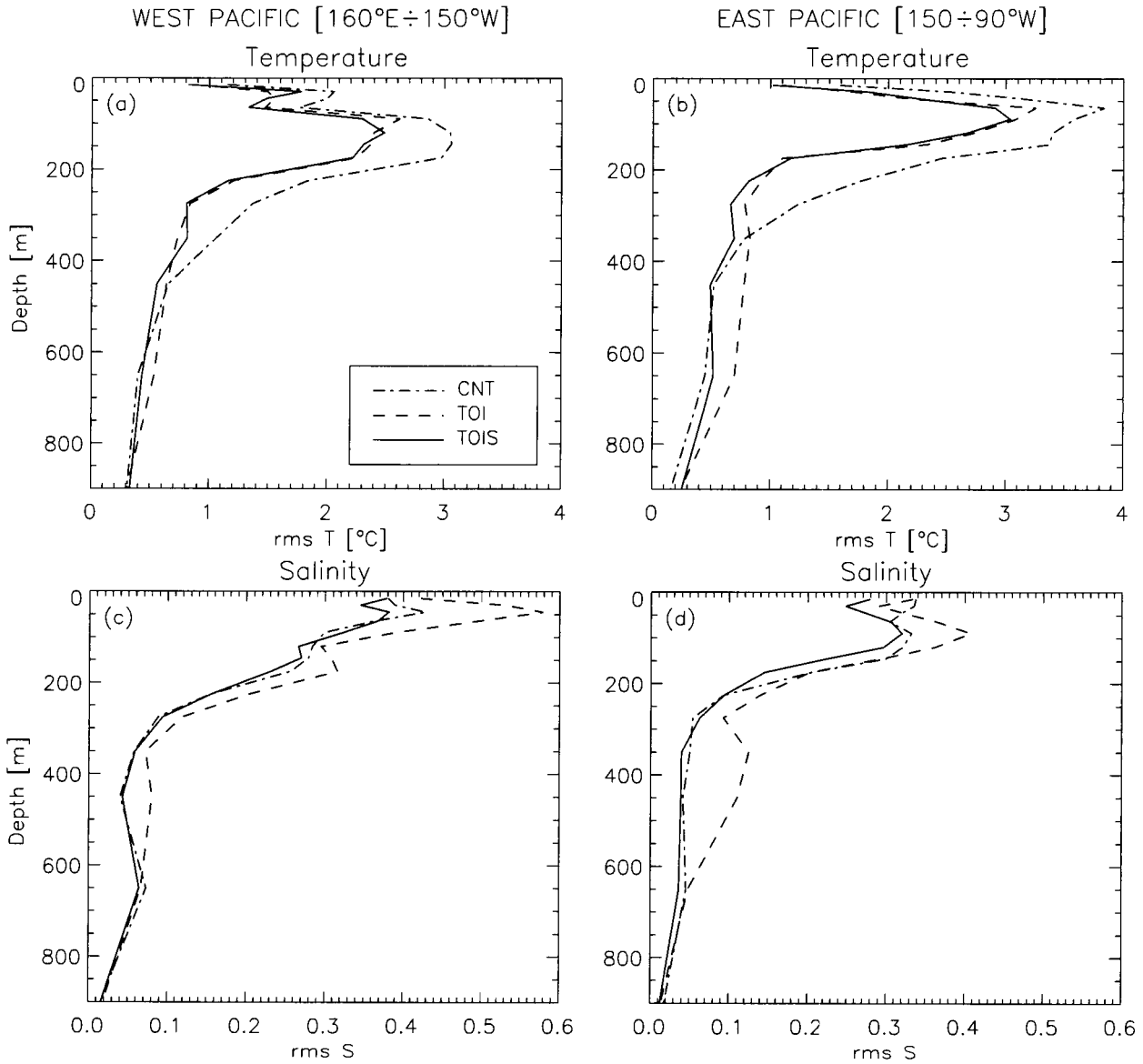


Figure 6: Root-mean-square difference (RMSD) between the three model runs (*TOI*, *TOIS* and *CNT*) and the observations as a function of depth for the 69 available transects in Figure 3: west equatorial Pacific (a, c) and east equatorial Pacific (b, d); temperature RMSD (a-b) and salinity RMSD (c-d).

It is very encouraging that the salinity RMSD in *TOIS* is systematically smaller than in *TOI* in both the EEP and the WEP (Figures 6c, d). Their difference reaches a peak of 0.16 at 50m in the WEP and 0.1 at 350m in the EEP. Note that below 250m in the EEP, the salinity RMSD trend largely reflects that for the temperature RMSD, again a consequence of the enhanced mixing which entrains saltier water at depth (see also the next section 3.3). The improvement of *TOIS* compared to *TOI* is relatively larger for salinity than for temperature. Considering the two regions, WEP and EEP, together, we obtain an average of 6% improvement for temperature and 20% for salinity. The salinity RMSD for *TOIS* is also marginally better than that for *CNT*, with an average improvement of 3%.

As mentioned above, the current structure is often also improved with TOIS. RMSD statistics calculated using ADCP observations for the EEP region showed an improvement in *TOIS* of 10% and 5% with respect to *TOI* and *CNT*, respectively. However, the improvements in zonal velocity are generally less than the uncertainty (5cm s^{-1}) in the observations.

3.3 Temperature-Salinity Relations

The detrimental impact of the *TOI* on the water-mass distribution is apparent in a comparison of *T-S* pairs for the observations, *TOI* and *TOIS*. Since the *T-S* characteristics differ between north and south of the equator, we further divide the two regions, EEP and WEP, considered above. We therefore account for four regions as presented in Figure 7.

The differences in *T-S* distributions between regions is clear from Figure 7. The *T-S* relation in the north WEP is generally tighter than in the other regions, with very little variation in salinity, but with a slight subsurface saline maximum associated with North Pacific Tropical Water (NPTW) and South Pacific Tropical Water (SPTW) which penetrates across the equator (see Johnson and McPhaden, 1999). The subsurface salinity maximum of the SPTW is a significant feature in the south WEP. In the south EEP, although the water is fresher at depth, the subsurface salinity maximum is less apparent because the surface waters are more saline in this region outside the South Pacific and Intertropical Convergence Zones. Hence, even in this narrow region, the TH99 scheme is tested in different *T-S* regimes.

Figure 7 is produced by considering the *T-S* pairs at each observation location and the model values interpolated to the observation locations. The *T-S* pairs are accumulated on a *T-S* grid whose granularity is 0.25°C by 0.1 . Where at least one *T-S* pair exists, a colored circle is plotted. This implies that each *T-S* grid point is given the same weight. However, by neglecting *T-S* grid points with a low occupancy number, we checked that the features shown in Figure 7 are robust.

The red color signifies that the *T-S* characteristics of all three ocean representations, *TOI*, *TOIS* and the observations, coincide. Manifestly, red is the predominant color in all four regions, implying that the two assimilation runs produce a good representation of the observed ocean. However, other features are also apparent. North of the equator (Figures 7a, b), the assimilation fields (as well as the control run, not shown) have fresher values than observations as seen from the abundance of violet circles for low salinities and, concurrently, from the cyan circles on the higher salinity range. These values mostly relate to fresher surface waters, often mixed into the upper thermocline (see the sections at 155°W for example) and result from deficiencies in the surface freshwater flux. In the north EEP, the fresher north Pacific influence in the model is also apparent. The few cyan circles in the figures for the northern hemisphere also indicate model deficiencies: in the penetration of NPTW equatorward in the WEP, and in the cross-equatorial penetration of SPTW in both WEP and EEP. There are very few black circles to indicate problems in the North Equatorial Pacific. In this region, variations in salinity in the equatorial waveguide are mainly in the surface layer, so there is little that the TH99 scheme can (or has to) do to rectify the model's salinity as the temperature is changed through assimilation.

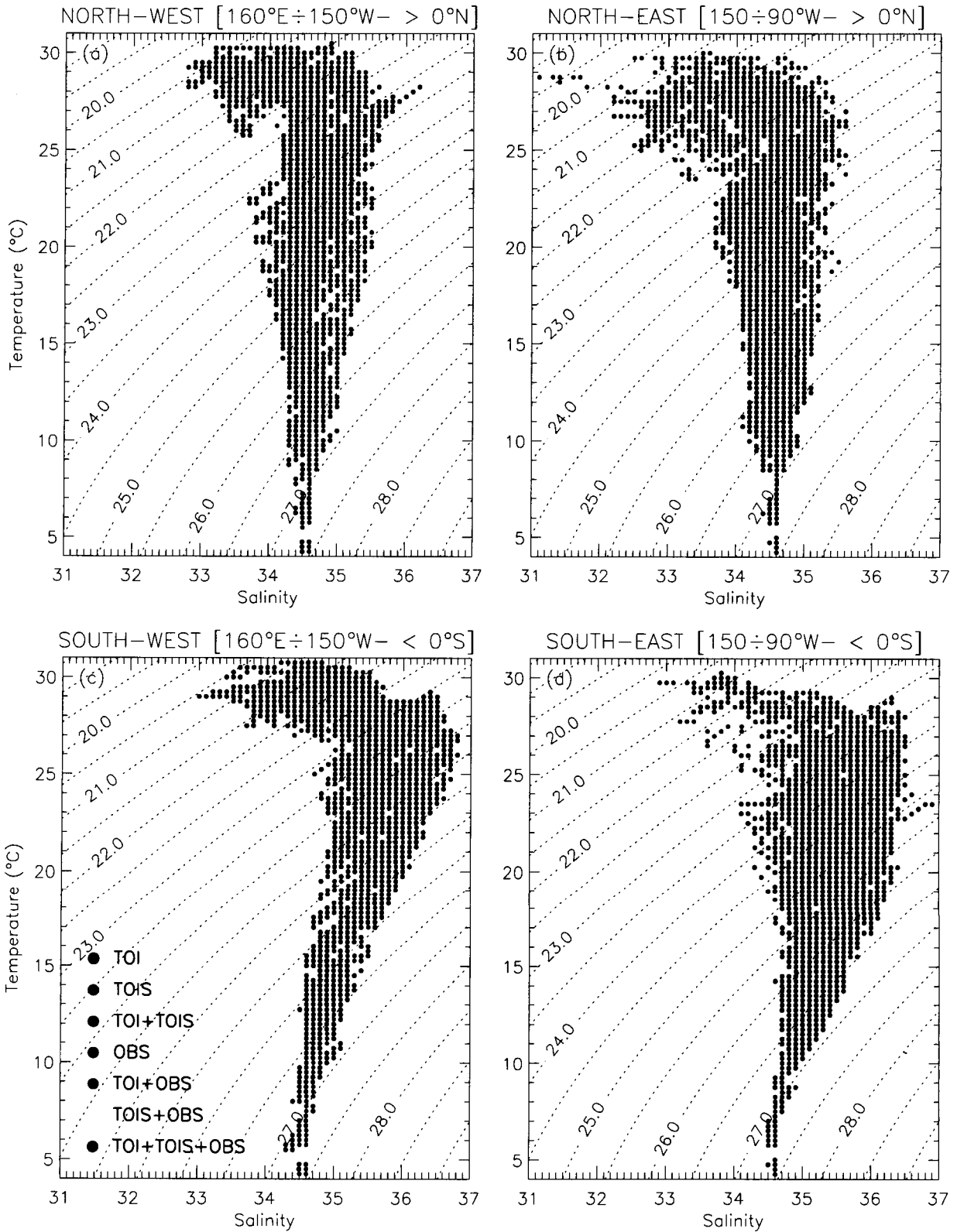


Figure 7: Temperature-Salinity diagrams for *TOI*, *TOIS* and observations (*OBS*) for the four regions defined on each panel. The color convention is explained in panel c. For instance, the red color means that both *TOI* and *TOIS* agree with observations. Superimposed dotted lines are the σ_t isolines.

South of the equator the representation of T - S in the $TOIS$ model is quite good (Figures 7c, d). On the other hand, a significant volume of cool, saline water is readily apparent in the TOI fields, as shown by the numerous black circles. These circles show that the problems associated with the univariate assimilation of temperature with no salinity correction are most significant in the southeastern Tropical Pacific. However, in the western basin (north and south) black circles are also noticeable on the fresh side of the T - S pairs.

4. Data Retention

The obvious question arises as to whether the improved states from $TOIS$ have any impact on seasonal forecast skill. As an initial attempt at answering this question, we have conducted forced ocean experiments, to be regarded as simulated forecast experiments, but with “perfect” surface forcings. These experiments have the advantage of avoiding the problem of initialization shocks and drifts of coupled ocean-atmosphere forecasts. The assimilation fields are used as initial conditions for the simulation, but after initialization no further assimilation has been undertaken. The experiments thus measure the retention of the information provided by assimilation and whether the undesirable features of the TOI states impact the subsequent ocean evolution or are ameliorated by ocean forcing and mixing. The error statistics from these simulations are compared with those from a pure simulation mode (the control) and from the continued assimilation case. These simulated forecast experiments were taken from the six April 1 dates of 1993 to 1998 and, in each case, are integrated for a six month duration.

We analyze the results of these forecasts by means of two diagnostics. The first uses RMSD as in Figure 6, whereas the second considers the RMSD for two specific subsurface variables as a function of lead time.

The RMSD diagnostic as a function of depth is shown in Figure 8 and now includes only the 35 transects that fall within the 6-month forecast interval, April to September (crossed transects in Figure 3). All the months have equal weighting in the RMSD calculation. The simulated forecasts initialized by TOI ($TOIS$) analyses are labeled as f_TOI , (f_TOIS). The overall results are hardly distinguishable from those in Figure 6, indicating that the information in the initial conditions is retained for at least 6 months. Only at thermocline depths in the EEP is there a notable increase in the RMSD by about 0.2°C for both f_TOI and f_TOIS , compared to TOI and $TOIS$, respectively (Figure 8b). Encouragingly, the f_TOIS salinity RMSD almost overlaps that for $TOIS$, implying that the subsurface information is retained on the timescales considered. The same holds true for the f_TOI - TOI pair, but as for the assimilation runs, the absolute RMSD values are markedly larger than for the f_TOIS - $TOIS$ pair.

To investigate the evolution of the errors with time, we analyzed the RMSD for the depth of the 19°C isotherm depth (Figures 9a, b) and for the salinity on the 25 sigma-theta surface (Figures 9c, d). These variables were chosen because, unlike the 20°C isotherm and the 24.5 sigma-theta surface representing the equatorial thermocline, they do not outcrop in the 35 transects. Over the six-month lead times, the 35 transects are thus distributed: 5, 6, 2, 4, 7 and 11. Ultimately, without further assimilation, the states from f_TOI , f_TOIS , and CNT would eventually evolve to be quite similar (within predictability limits).

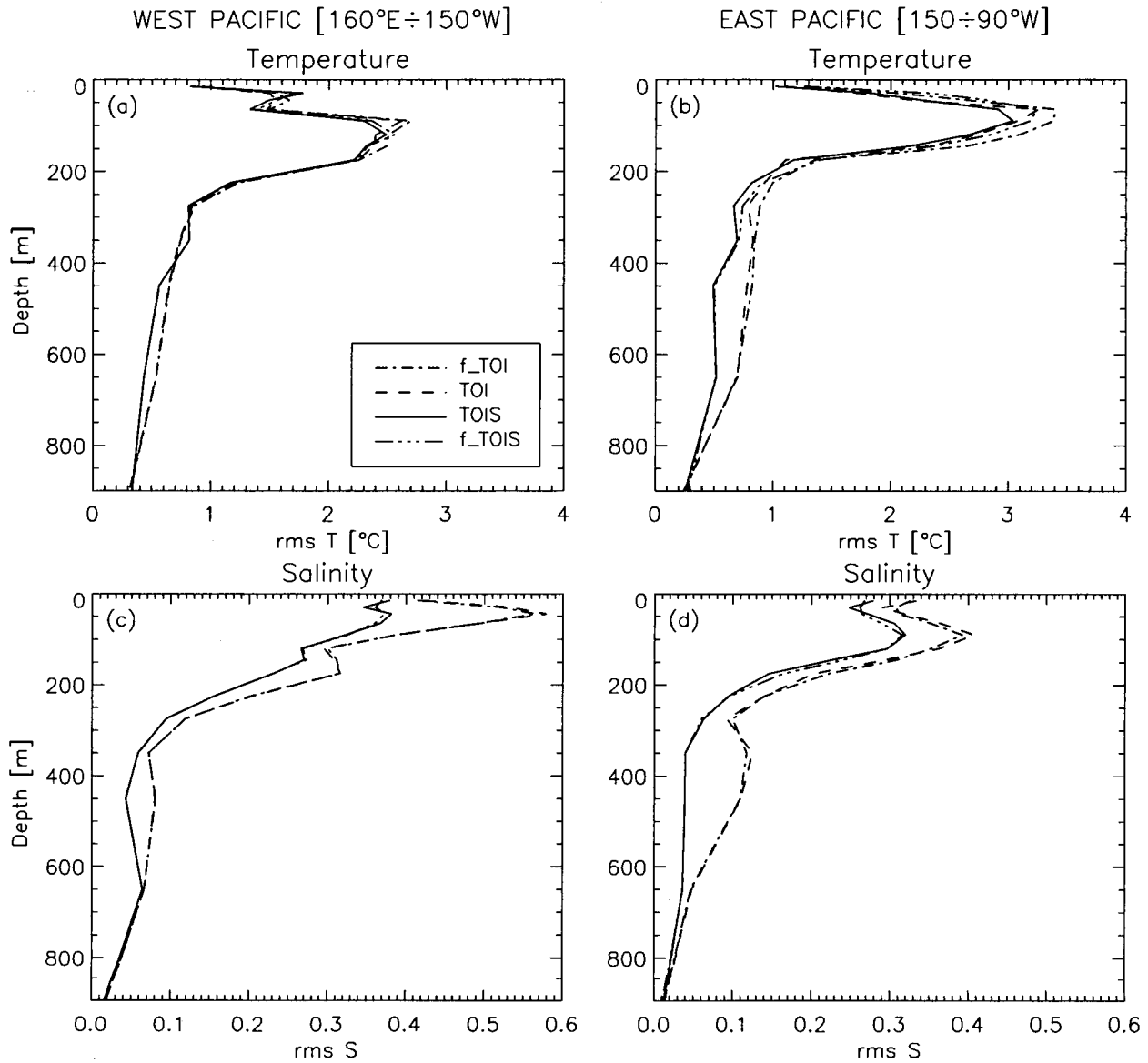


Figure 8: As in Figure 6 but for the two assimilation runs, *TOI* and *TOIS*, and the two simulated forecasts, *f_TOI* and *f_TOIS*, and for the 35 crossed transects (see Figure 3).

However, figure 5 clearly shows that the improved initial conditions provided by both assimilations are retained for at least six months. The *TOI* states produce a better simulation than the control, except for the salinity north of the equator. The improved state resulting from *TOIS* is also generally retained throughout the forecast period, so we conclude that the correction of subsurface salinity should have a positive impact on seasonal forecast skill. South of the equator, the improvements in the state estimate are retained for six months and generally the salinity errors introduced by *TOI* seem to be ameliorated somewhat once the assimilation is stopped. North of the equator, however, the errors in salinity introduced by the assimilation persist through the six-

month period. This would indicate that direct salinity observations north of the equator would be beneficial.

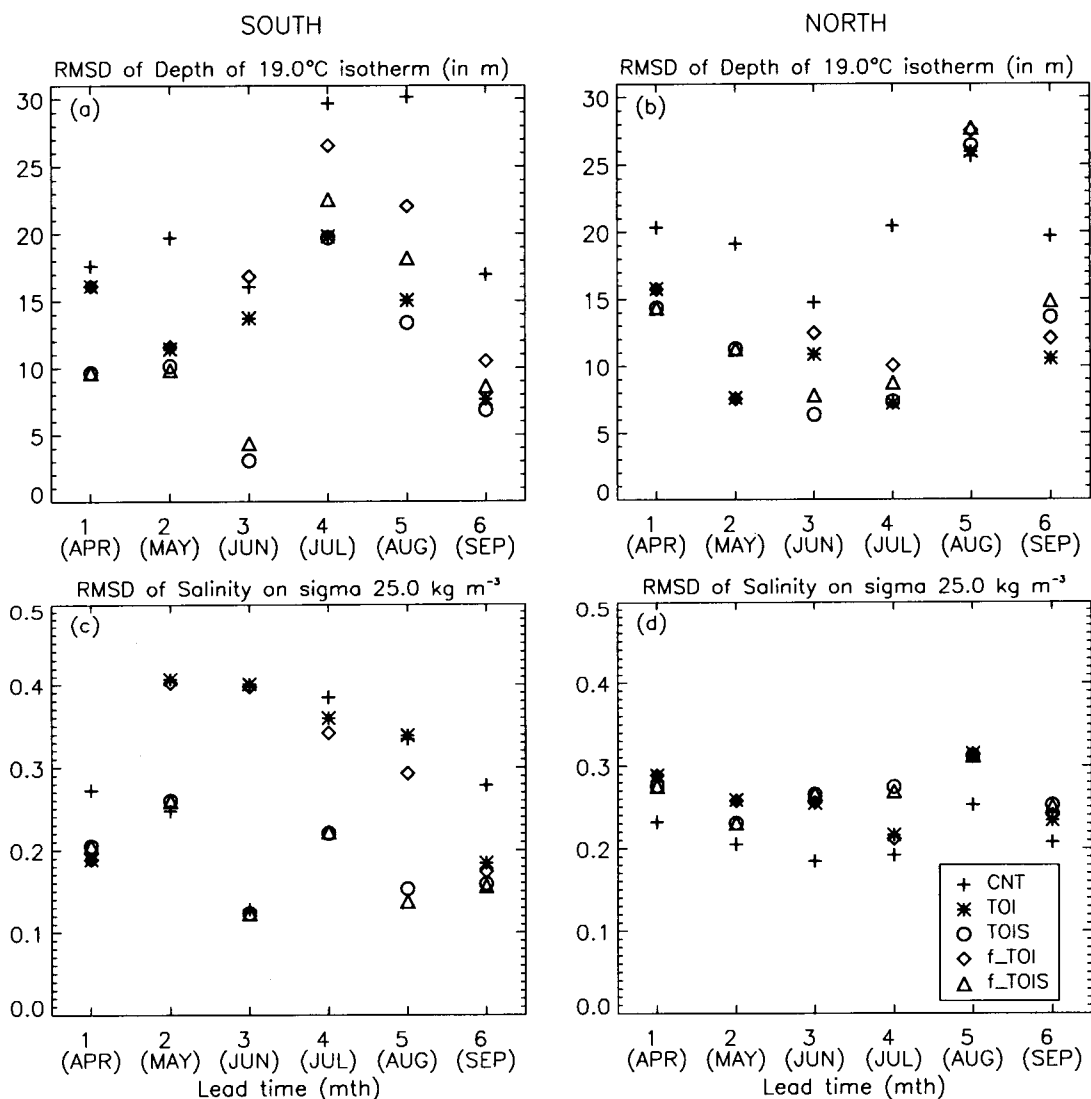


Figure 9. Temporal evolution of the composite RMSD of the 19°C isotherm depth (a-b) and of the salinity on the 25 sigma surface (c-d) for all lead times for the control run (CNT), the two assimilation runs (TOI and TOIS), and the simulated forecasts (f_TOI and f_TOIS). The RMSD calculation is split in south (a, c) and north (b, d) of the equator.

5. Summary and discussion

The general applicability of the salinity correction scheme documented in TH99 and TBS02 is tested here in an isopycnal model rather than a z-coordinate model. The scheme is validated more stringently by comparison with a large volume of time-varying temperature and salinity observations collected along 69 transects across the equatorial Pacific over the 6-year period 1993-1998 (Johnson *et al.*, 2000, plus subsequent extension). This scheme has been implemented in the data assimilation system employed for NSIPP's routine forecasts.

Even within the equatorial waveguide, the TH99 scheme is tested in different *T-S* configurations, with variations in salinity structure across the equator and along the equator as seen in Johnson and McPhaden (1999). The root-mean-square differences between the assimilation estimates of the salinity and temperature fields and these observations offer an encouraging assessment of the salinity-correction scheme when compared to a conventional OI procedure that does not update salinity. For instance, the improvement in the salinity field is 20% when the TH99 scheme is used compared to when only the temperature field is updated. Another evaluation that was carried out with this work is that of the impact of subsurface initializations on simulated forecasts. We showed that both the subsurface salinity and temperature benefit from the TH99 scheme for all lead times considered (up to 6 months) in the south equatorial Pacific. The north equatorial Pacific has proven to be a more difficult region to improve, given the presence of systematic errors in the model. It is perhaps this region that could most benefit from direct salinity observations. Whether the TH99 salinity scheme performs better than other approaches such as multivariate OI, based on observations (e.g., Maes and Behringer, 2000) or model-based covariances, or the Ensemble Kalman Filter is a matter that will be assessed in the near future. It is apparent though that, given its simplicity, the TH99 scheme is effective and easily implemented in any ocean model. Also, it does not need any observation or model climatology that can limit the variation spread. However, the TH99 scheme strongly relies on the model dynamics to get a good salinity field reconstruction and therefore it can only be applied to ocean models that simulate the distribution of water masses reasonably well. It has been shown in this study, as well as in TBS02, that the two primitive equation models in question, Poseidon and HOPE, satisfy this requirement well (although improvements are needed in the northern equatorial Pacific). It might also be argued that the success of such a simple scheme lies in its aim of preserving the density balances - through the conservation of the isopycnal layering - present in the model prior to assimilation. It appears that initializing the model with a balanced density field is crucial in a sequential data assimilation framework. The TH99 scheme could therefore be employed by even more complex assimilation systems for initialization purposes.

Acknowledgements

Computer time was provided by the NASA Center for Computational Sciences at NASA/Goddard Space Flight Center. This research was supported by RTOP 622-48-04 from the NASA Physical Oceanography Research and Analysis Program. GCJ was supported by the NOAA Office of Oceanic and Atmospheric Research, the NOAA Office of Global Programs, and the NASA Physical Oceanography Program. Temperature observations for assimilation were quality controlled and provided by Dr. David Behringer at NCEP.

References

- Acero-Schertzer, C. E., D. V. Hansen, and M. S. Swenson, 1997: Evaluation and diagnosis of surface currents in the National Centers for Environmental Prediction's ocean analyses, *J. Geophys. Res.*, **102**, 21 037-21 048.
- Atlas, R., R. Hoffman, S. Bloom, J. Jusem, and J. Ardizzone, 1996: A multiyear global surface wind velocity dataset using SSM/I wind observations. *Bull. Amer. Met. Soc.*, **77**, 869-882.
- Bloom, S., L. Takacs, A. DaSilva, and D. Ledvina, 1996: Data assimilation using incremental analysis updates. *Mon. Wea. Rev.*, **124**, 1256-1271.
- Borovikov, A., M. M. Rienecker, and P. Schopf, 2001: Surface heat balance in the Equatorial Pacific Ocean: climatology and the warming event of 1994-95. *J. Clim.*, **14**, 2624-2641.
- Coles, V. J. and M. M. Rienecker, 2001: North Pacific subtropical-tropical gyre exchanges in the thermocline: Simulations with two isopycnic OGCMs, *J. Phys. Oceanogr.*, **31**, 2590-2611.
- Cooper, N., 1988: The effect of salinity on tropical ocean models, *J. Phys. Oceanogr.*, **18**, 697-707.
- Daley, R., 1991: *Atmospheric Data Analysis*. Cambridge University Press, 457pp.
- Derber, J. and A. Rosati, 1989: A global oceanic data assimilation system, *J. Phys. Oceanogr.*, **19**, 1333-1347.
- Ji, M., D. W. Behringer, and A. Leetmaa, 1998: An improved coupled model for ENSO prediction and implications for ocean initialization. Part II: The coupled model, *Mon. Wea. Rev.*, **126**, 1022-1034.
- Ji, M., A. Leetmaa, and J. Derber, 1995: An ocean analysis system for seasonal to interannual climate studies, *Mon. Wea. Rev.*, **123**, 460-481.
- Ji, M., R. W. Reynolds, and D. W. Behringer, 2000: Use of TOPEX/Poseidon sea level data for ocean analyses and ENSO prediction: Some early results, *J. Climate*, **13**, 216-231.
- Johnson, G. C. and M. J. McPhaden, 1999: Interior pycnocline flow from the subtropical to the equatorial Pacific ocean, *J. Phys. Oceanogr.*, **29**, 3073-3089.
- Johnson, G. C., M. J. McPhaden, G. D. Rowe, and K. E. McTaggart, 2000: Upper equatorial Pacific ocean current and salinity variability during the 1996-1998 El Niño-La Niña cycle, *J. Geophys. Res.*, **105**, 1037-1053.

- Keppenne, C. L. and M. M. Rienecker, 2002: Design and implementation of a massively parallel multivariate ensemble Kalman filter for the Poseidon ocean general circulation model, *Mon. Wea. Rev.*, **130**, 2951-2965.
- Keppenne, C.L. and M. M. Rienecker, 2001: Design and implementation of a parallel multivariate ensemble Kalman Filter for the Poseidon ocean general circulation model. NASA Tech. Memo-2001-104606, NASA Tech. Rep. Series on Global Modeling and Data Assimilation, Vol 21., 35pp.
- Konchady, M., A. Sood, and P. Schopf, 1998: Implementation and performance evaluation of a parallel ocean model. *Parallel Comput.*, **24**, 181-203.
- Lorenc, A., 1981: A global three-dimensional multivariate statistical interpolation scheme, *Mon. Wea. Rev.*, **108**, 701-721.
- Maes, C. and D. W. Behringer, 2000: Using satellite-derived sea level and temperature profiles for determining the salinity variability: A new approach, *J. Geophys. Res.*, **105**, 8537-8547.
- McPhaden, M. J., A. Busalacchi, R. Cheney, J. Donguy, K. S. Gage, D. Halpern, M. Ji, P. Julian, G. T. Meyers, P. P. Niiler, J. Picant, R. W. Reynolds, N. Smith, and K. Tekeuchi, 1998: The tropical ocean global atmosphere observing system: A decade of progress, *J. Geophys. Res.*, **103**, 14169-14240.
- Niiler, P. P. and E. B. Kraus, 1977: *One-dimensional models of the upper ocean*, Modeling and prediction of the upper layers of the ocean, edited by E. B. Kraus, Ed. Pergamon, pp. 143-172.
- Pacanowski, R. C. and S. G. H. Philander, 1981: Parameterization of vertical mixing in numerical models of the tropical oceans, *J. Phys. Oceanogr.*, **11**, 1443-1451.
- Schaffer, D. and M. Suarez, 2000: Design and performance analysis of a massively parallel atmospheric general circulation model, *Scientific Prog.*, **8**, 49-57.
- Schopf, P. S. and A. Loughe, 1995: A reduced-gravity isopycnal ocean model: Hindcasts of El Niño, *Mon. Wea. Rev.*, **123**, 2839-2863.
- Seager, R., M. B. Blumenthal, and Y. Kushnir, 1995: An advective atmospheric mixed layer model for ocean modeling purposes: Global simulation of surface heat fluxes, *J. Climate*, **8**, 1951-1964.
- Segschneider, J., D. L. T. Anderson, J. Vialard, M. Balmaseda, T.N. Stockdale, A. Troccoli, and K. Haines, 2001: Initialization of seasonal forecasts assimilating sea level and temperature observations, *J. Climate*, **14**, 4292-4307.
- Troccoli, A. and K. Haines, 1999: Use of the Temperature-Salinity relation in a data assimilation context, *J. Atmos. Oceanic Technol.*, **16**, 2011-2025.

- Troccoli A., M. Balmaseda, J. Segnschneider, J. Vialard, D. Anderson, K. Haines, T. Stockdale, F. Vitart, and A. D. Fox, 2002: Salinity adjustments in the presence of temperature data assimilation, *Mon. Wea. Rev.*, **130**, 89-102.
- Vossepoel, F. C. and D. W. Behringer, 2000: Impact of sea level assimilation on salinity variability in the western equatorial Pacific, *J. Phys. Oceanogr.*, **30**, 1706-1721.
- Vossepoel, F. C., R. W. Reynolds, and L. Miller, 1999: Use of sea level observations to estimate salinity variability in the tropical Pacific, *J. Atmos. Oceanic Technol.*, **16**, 1401-1415.
- Xie, P. P. and P. Arkin, 1997: Global precipitation: A 17-year monthly analysis based on gauge observations, satellite estimates, and numerical model outputs, *B. Am. Meteorol. Soc.*, **11**, 2539-2558.
- Yang, S., K. Lau, and P. Schopf, 1999: Sensitivity of the tropical Pacific Ocean to precipitation induced freshwater flux, *Clim. Dynam.*, **15**, 737-750.

Previous Volumes in This Series

- Volume 1**
September 1994
Documentation of the Goddard Earth Observing System (GEOS) general circulation model –Version 1.
L.L. Takacs, A. Molod, and T. Wang
- Volume 2**
October 1994
Direct solution of the implicit formulation of fourth order horizontal diffusion for gridpoint models on the sphere
Y. Li, S. Moorthi, and J.R. Bates
- Volume 3**
December 1994
An efficient thermal infrared radiation parameterization for use in general circulation models
M.-D. Chou and M.J. Suarez
- Volume 4**
January 1995
Documentation of the Goddard Earth Observing System (GEOS) Data Assimilation System – Version 1.
James Pfaendtner, Stephen Bloom, David Lamich, Michael Seablom, Meta Sienkiewicz, James Stobie, and Arlindo da Silva
- Volume 5**
April 1995
Documentation of the Aries-GEOS dynamical core: Version 2.
Max J. Suarez and Lawrence L. Takacs
- Volume 6**
April 1995
A Multiyear Assimilation with the GEOS-I System: Overview and Results
Siegfried Schubert, Chung-Kyu Park, Chung-Yu Wu, Wayne Higgins, Yelena Kondratyeva, Andrea Molod, Lawrence Takacs, Michael Seablom, and Richard Rood
- Volume 7**
September 1995
Proceedings of the Workshop on the GEOS-I Five-Year Assimilation
Siegfried D. Schubert and Richard B. Rood
- Volume 8**
March 1996
Documentation of the Tangent Linear Model and its Adjoint of the Adiabatic Version of the NASA GEOS-I C-Grid GCM: Version 5.2
Weiyu Yang and I. Michael Navon
- Volume 9**
March 1996
Energy and Water Balance Calculations in the Mosaic LSM
Randal D. Koster and Max J. Suarez
- Volume 10**
April 1996
Dynamical Aspects of Climate Simulations Using the GEOS General Circulation Model
Lawrence L. Takacs and Max J. Suarez

- Volume 11**
May 1997
Documentation of the Tangent Linear and its Adjoint Models of the Relaxed Arakawa-Schubert Moisture Parameterization Package of the NASA GEOS-I GCM – Version 5.2
Weiyu Yang I, Michael Navon, and Ricardo Todling
- Volume 12**
August 1997
Comparison of Satellite Global Rainfall Algorithms
Alfred T.C. Chang and Long S. Chiu
- Volume 13**
December 1997
Interannual Variability and Potential Predictability in Re-Analysis Products
Wie Ming and Siegfried D. Schubert
- Volume 14**
August 1998
A Comparison of GEOS Assimilated Data with FIFE Observations
Michael G. Bosilovich and Siegfried D. Schubert
- Volume 15**
June 1999
A Solar Radiation Parameterization for Atmospheric Studies
Ming-Dah Chou and Max J. Suarez
- Volume 16**
November 1999
Filtering Techniques on a Stretched Grid General Circulation Model
Lawrence Takacs, William Sawyer, Max J. Suarez, and Michael S. Fox-Rabinowitz
- Volume 17**
July 2000
Atlas of Seasonal Means Simulated by the NSIPP-1 Atmospheric GCM
Julio T. Bacmeister, Philip J. Pegion, Siegfried D. Schubert, and Max J. Suarez
- Volume 18**
December 2000
An Assessment of the Predictability of Northern Winter Seasonal Means with the NSIPP-1 AGCM
Philip J. Pegion, Siegfried D. Schubert, and Max J. Suarez
- Volume 19**
July 2001
A Thermal Infrared Radiation Parameterization for Atmospheric Studies
Ming-Dah Chou, Max J. Suarez, Xin-Zhong, Michael M.-H. Yan
- Volume 20**
August 2001
The Climate of the FVCCM-3 Model
Yehui Chang, Siegfried D. Schubert, Shian-Jiann Lin, Sharon Nebuda, Bo-Wen Shen
- Volume 21**
September 2001
Design and Implementation of a Parallel Multivariate Ensemble Kalman Filter for the Poseidon Ocean General Circulation Model
Christian L. Keppenne and Michele M. Rienecker

Volume 22
August 2002

**A Coupled Ocean-Atmosphere Radiative Model for Global
Ocean Biogeochemical Models
Watson W. Gregg**

Volume 23
November 2002

**Prospects for Improved Forecasts of Weather and Short-Term
Climate Variability on Subseasonal (2-Week to 2-Month) Time
Scales
Sigfried D. Schubert, Randall Dole, Huang van den Dool,
Max J. Suarez, and Duane Waliser**

REPORT DOCUMENTATION PAGEForm Approved
OMB No. 0704-0188

Public reporting burden for this collection of information is estimated to average 1 hour per response, including the time for reviewing instructions, searching existing data sources, gathering and maintaining the data needed, and completing and reviewing the collection of information. Send comments regarding this burden estimate or any other aspect of this collection of information, including suggestions for reducing this burden, to Washington Headquarters Services, Directorate for Information Operations and Reports, 1215 Jefferson Davis Highway, Suite 1204, Arlington, VA 22202-4302, and to the Office of Management and Budget, Paperwork Reduction Project (0704-0188), Washington, DC 20503.

1. AGENCY USE ONLY (Leave blank)		2. REPORT DATE July 2003	3. REPORT TYPE AND DATES COVERED Technical Memorandum	
4. TITLE AND SUBTITLE Temperature Data Assimilation with Salinity Corrections: Validation for the NSIPP Ocean Data Assimilation System in the Tropical Pacific Ocean, 1993-1998			5. FUNDING NUMBERS Code 971	
6. AUTHOR(S) Alberto Troccoli, Michele M. Rienecker, Christian L. Keppenne, Gregory C. Johnson,				
7. PERFORMING ORGANIZATION NAME(S) AND ADDRESS (ES) Goddard Space Flight Center Greenbelt, Maryland 20771			8. PERFORMING ORGANIZATION REPORT NUMBER 2003-02419-0	
9. SPONSORING / MONITORING AGENCY NAME(S) AND ADDRESS (ES) National Aeronautics and Space Administration Washington, DC 20546-0001			10. SPONSORING / MONITORING AGENCY REPORT NUMBER TM-2003-104606, Vol. 24	
11. SUPPLEMENTARY NOTES Christian L. Keppenne, SAIC, Beltsville, MD; Gregory C. Johnson, NOAA, Seattle, WA				
12a. DISTRIBUTION / AVAILABILITY STATEMENT Unclassified-Unlimited Subject Category: 42 Report available from the NASA Center for AeroSpace Information, 7121 Standard Drive, Hanover, MD 21076-1320. (301) 621-0390.			12b. DISTRIBUTION CODE	
13. ABSTRACT (Maximum 200 words) The NASA Seasonal-to-Interannual Prediction Project (NSIPP) has developed an ocean data assimilation system to initialize the quasi-isopycnal ocean model used in our experimental coupled-model forecast system. Initial tests of the system have focused on the assimilation of temperature profiles in an optimal interpolation framework. It is now recognized that correction of temperature only often introduces spurious water masses. The resulting density distribution can be statically unstable and also have a detrimental impact on the velocity distribution. Several simple schemes have been developed to try to correct these deficiencies. Here the salinity field is corrected by using a scheme which assumes that the temperature-salinity relationship of the model background is preserved during the assimilation. The scheme was first introduced for a zlevel model by Troccoli and Haines (1999). A large set of subsurface observations of salinity and temperature is used to cross-validate two data assimilation experiments run for the 6-year period 1993-1998. In these two experiments only subsurface temperature observations are used, but in one case the salinity field is also updated whenever temperature observations are available.				
14. SUBJECT TERMS NASA Seasonal-to-Interannual Prediction Project (NSIPP)			15. NUMBER OF PAGES 26	
			16. PRICE CODE	
17. SECURITY CLASSIFICATION OF REPORT Unclassified	18. SECURITY CLASSIFICATION OF THIS PAGE Unclassified	19. SECURITY CLASSIFICATION OF ABSTRACT Unclassified	20. LIMITATION OF ABSTRACT UL	